Available online at www.sciencedirect.com
SCIENCE DIRECT
Thermochimica Acta 446 (2006) 168–175
thermochimica acta
www.elsevier.com/locate/tca

Chip calorimeters for the investigation of liquid phase reactions: Design rules

J. Lerchner [a,*], A. Wolf [a], G. Wolf [a], I. Fernandez [b]

[a] *Institut f. Physikalische Chemie, TU Bergakademie Freiberg, Leipziger Str. 29, D-09596 Freiberg/Sachsen, Germany*
[b] *CIRG-DF A-ETSECCPB, Polytechnical University of Catalonia, Campus Nord B-4, E-08034 Barcelona, Spain*
Available online 10 May 2006

Dedicated to Professor Wolfgang Hemminger on the occasion of his 65th anniversary

Abstract

Rules for the design of silicon chip based devices for liquid phase calorimetry are discussed. In contrast to the study of fast reactions the investigation of slow processes like the metabolic heat production requires sample volumes of at least a few micro-liters if a signal resolution in the $mW\,l^{-1}$ range is necessary. On the other hand, increasing sensitivity gradients inside the reaction chamber and external temperature perturbations restrict its enlargement. Therefore, a careful optimization of the device with respect to the sample volume is necessary if one likes to use the advantages of chip calorimeters. The presented study was performed by use of a new designed flow-through chip calorimeter.

Keywords: Chip calorimetry; Heat transfer; Calorimeter simulation; Models; Accuracy

1. Introduction

During the last decade it was demonstrated that chip calorimetry can be applied with considerable gain in various fields of chemical and physical research. Most benefit is obtained if fast and transient processes are investigated. For given concentrations of the reactants and enthalpy of reaction the signal-to-noise ratio (SNR) only depends on the sensitivity of the temperature transducer and less on the sample volume if the reaction is fast in comparison with the time constant of the device Eq. (1). As a consequence, samples of extremely small size can be investigated. The reason is the small heat capacity of the addenda (<1 $mJ\,K^{-1}$), which is essentially the feature of chip calorimeters.

$$\mathrm{SNR} = \frac{\Delta u}{u_n} = \frac{S_T \Delta T_{ad}}{u_n} = \frac{S_T}{u_n}\frac{q}{C} = \frac{S_T}{u_n}\frac{cV\Delta H}{\rho c_p V + C_a} \approx \frac{S_T}{u_n}\frac{c\Delta H}{\rho c_p} \quad (1)$$

In the above equation Δu and u_n are the measured signal and the voltage noise for a given band width, respectively. S_T is the sensitivity of the temperature transducer in $V\,K^{-1}$, ΔT_{ad} the adiabatic temperature change in K, q the dissipated amount of heat in J, C the total heat capacity in $J\,K^{-1}$, c the concentration of the reactants in $mol\,m^{-3}$, V the sample volume in m^3, ΔH the enthalpy of reaction in $J\,mol^{-1}$, ρ the density of the sample in $kg\,m^{-3}$, c_p the specific heat capacity of the sample in $J\,kg^{-1}\,K^{-1}$ and C_a is the heat capacity of the addenda in $J\,K^{-1}$. Examples for the investigation of extremely small samples are the measurement of peptide–ligand binding energies in nano-liter samples [1], the determination of heats of fusion of nano-sized clusters [2] and the calorimetrical study of absorption phenomena in thin coatings [3].

In the case of slow processes the heat capacity of the chip is of secondary importance and the SNR decreases in turn with the miniaturization of the sample.

$$\mathrm{SNR} = \frac{\Delta u}{u_n} = \frac{S_p p}{u_n} = \frac{S_p}{u_n} r V \Delta H \quad (2)$$

Here, S_p is the heat power sensitivity (transfer of the calorimeter chip) in $V\,W^{-1}$, p the dissipated heat power in W and r is the rate of reaction in $mol\,m^{-3}\,s^{-1}$. Also the volume related heat power detection limit, $\sigma_{p,V}$, which is proportional to the inverse of the SNR, can be used for the characterization of the detecting performance of the device Eq. (3).

$$\sigma_{p,V} = \frac{u_n}{S_p V} \quad (3)$$

* Corresponding author. Tel.: +49 3731 392125; fax: +49 3731 393588.
E-mail address: Johannes.Lerchner@chemie.tu-freiberg.de (J. Lerchner).

0040-6031/$ – see front matter © 2006 Elsevier B.V. All rights reserved.
doi:10.1016/j.tca.2006.04.020

Because of the decrease of the SNR with reducing of the sample size, a favorable application of chip calorimeters becomes questionable. Despite of the considerable large heat power sensitivity, which can be obtained for silicon thermopile chips (>10 V W^{-1} [4]), chip calorimeters will never compete with conventional ones in the SNR under these conditions. On the other hand, there is a large potential for the application of miniaturized calorimeters in microbiology and biochemistry, where small samples have to be studied. Also the use of miniaturized calorimeters as control device in biotechnological processes could be of interest [5]. In most cases more or less steady-state processes have to be monitored. Therefore, the size of the calorimeter must be optimized. For relevant applications in biochemistry or microbiology the volume related heat power resolution $\sigma_{p,V}$ should not exceed a few mW l^{-1}. With a heat power resolution of 100 nW a sample volume of 10 μl is required if a specific heat power resolution of 10 mW l^{-1} is demanded. Extremely miniaturized calorimeters are useful only for very specialized applications (Johannessen et al. [6]: V = 780 pl, $\sigma_{p,V}$ = 18 W l^{-1}, Zhang and Tadigadapa [7]: V = 15 nl, $\sigma_{p,V}$ = 6 W l^{-1}).

In the presented work we intend to discuss some aspects concerning the optimal design of chip calorimeters which can be applied in liquid phase reaction calorimetry of micro-liter samples:

- Convective heat loss due to reduced residence time.
- Incomplete conversion of the reactants caused by slow diffusive mixing and small rate of reaction.
- Systematic errors due to incomplete integration of the dissipated heat power.
- Influence of external temperature fluctuations on the signal-to-noise ratio.

Because of their practical relevance our considerations will be focused on flow-through devices. The study is based on experiments performed with a new flow-through chip calorimeter which was recently published [8]. The presented analysis of the considered flow-through chip calorimeter is in turn with a series of papers providing a general study of systematic errors in chip calorimeters [9–11].

2. Experimental

2.1. The calorimetric device

Fig. 1 depicts a photograph and the scheme of the calorimetric chip module, which is the heat power detector of the flow-through chip calorimeter and which was used for our investigations [8]. In order to study the influence of the sample volume on the performance of the calorimeter the height of the reaction chamber was varied. At a fixed length of the channel (20 mm) the used chamber heights of 0.6, 0.8 and 1.2 mm correspond to sample volumes of 12, 16 and 24 μl, respectively. The average

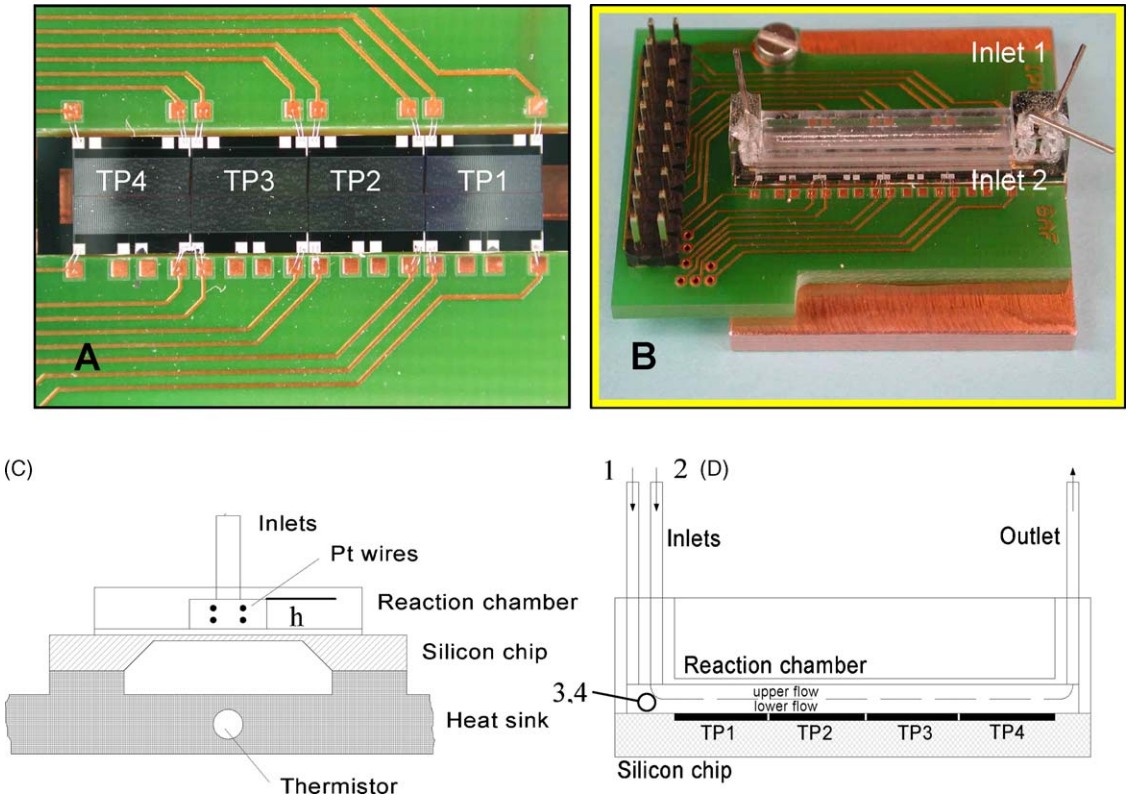

Fig. 1. Calorimetric chip module. (A) Bonded thermopile silicon chip with four thermopile segments in line (TP1–TP4). (B) Complete module consisting of the silicon chip, the PMMA reaction chamber and the copper heat sink. (C) Schematic cross section of the module. Two platinum wires are mounted in a loop at different positions. (D) Schematic side view of the reaction chamber with the hypothetical laminar reactant flows. Inlets 3 and 4 exist only for 1.2 mm chambers.

height of every chamber was determined by measuring the volume in the thermopile section with an accuracy of 2%. In the case of the 1.2 mm reaction chamber two different inlet positions were used to modify the local orientation of the laminar reactant flows inside the reaction chamber. For this two vertical (1, 2) and two horizontal (3, 4) inlet tubes are attached. For the sensitivity studies a calorimetric module was prepared with a 1.7 mm reaction chamber and two platinum wires inside (Fig. 1C). The wires were used for Joule heating experiments in addition to the four integrated thin film heaters. Measurements at different positions of the wires should provide information about sensitivity changes orthogonal to the detector membrane. The temperature sensor which is located inside the copper heat sink of the calorimetric module (Fig. 1C) served for measuring of external temperature disturbances. Temperature perturbations were generated by a stochastic modulation of the set point temperature of the thermostat.

2.2. Sensitivity measurements

Calorimetric sensitivities were determined by Joule heating experiments and by applying appropriate chemical reactions. In order to study the influence of the thermal properties of different liquids Joule heating experiments based on the integrated thin film heaters were performed with water, ethanol and butanol. Sensitivity data were derived from steady-state signals obtained as a function of the Joule heating power. The Joule heating measurements using the platinum wires were done only with water.

Two chemical calibration reactions of different kinetics were applied: the protonization of TRIS [12] and the base catalyzed hydrolysis of methylparaben (BCHMP) [13]. In the first case 0.1 M solution of TRIS and 0.02 M hydrochloric acid were simultaneously injected with equal flow rates through the two inlets. Steady-state signals were measured dependent on the flow rate in the range of 2.5–7.5 μl min^{-1} (Fig. 2). Calorimetric sensitivity data were derived from the slope using a protonization enthalpy of −47.4 kJ mol^{-1} [12]. In the axial direction the channel overlaps the thermopile segments by a few tenths of millimeter (Fig. 1D). Therefore, the reaction partially takes place before entering into the thermopile segments and, as a consequence, a fraction of the generated heat power cannot be detected, which is indicated by the intercept of the curve. Because the protonization is fast and laminar flows are expected, the rate of conversion is determined by the rate of diffusion of the reactants through the interface of the laminar flows. If differences in the diffusion coefficients exist different local orientations of the reactant flows should result in different heat power distributions. Hence, different average sensitivities are expected if there are sensitivity gradients inside the reaction chamber. For a proof of this assumed effect the reactants were injected through different inlets. The different injection modes are summarized in Table 1. Horizontal inlets could be attached only for 1.2 mm chambers due to geometric restrictions.

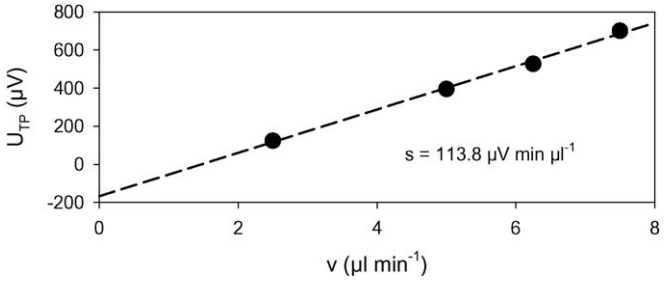

Fig. 2. Overall steady-state signals vs. flow rate for the continuous injection of HCl and TRIS solution into a 0.6 mm chamber (VB orientation).

Table 1
Injection modes used for the TRIS/HCl calibration reaction

	Inlet number	
	TRIS	HCl
VA	2	1
VB	1	2
HA	3	4
HB	4	3

In the case of the slow hydrolysis of methylparaben the reactants were mixed outside the calorimeter and 50 μl of the mixture (50 mM methylparaben in 0.5 M sodium hydroxide) were injected through one of the inlets. In contrast to the protonization of TRIS a homogeneously heat power dissipation can be expected. After injection of the mixture the decay of the heat power was measured for 90 min. Because the kinetic and thermodynamic data of the reaction are well known [13] a first order modeling of the time dependent signal change with respect to the time of mixing and the chamber volume provides the sensitivity of the calorimeter. For base line corrections the reaction mixture was replaced by injecting 0.5 M sodium hydroxide solution through the other inlet following each measurement.

3. Results and discussions

3.1. Degree of conversion and convective heat losses

Reduced residence time due to a small chamber volume and higher thermal resistance (>100 K W^{-1} in comparison with typically 2 K W^{-1} for a conventional flow-through calorimeter) induce the problem of convective heat loss and incomplete conversion of the reactants. In addition to small reaction rates slow diffusive mixing disables a complete conversion. In order to prevent related errors heats of reaction should be measured dependent on the flow rate. Then corrections could be applied [10].

A more reasonable way is to construct a reaction chamber with long size in flow direction and small thickness of the flow channel to provide short mass and thermal diffusion length. Independent heat power detectors which are distributed along the reaction chamber can give information about the completeness of conversion and heat exchange as it is the case in the device which we have used.

Nearly zero signals of TP4 (Fig. 3) indicate that in the applied range of flow rates a complete conversion and heat exchange is achieved for the TRIS protonization. If the diffusion of the protons is assumed as limiting quantity for the rate of conversion a residence time of 19 s is necessary for a layer thickness of

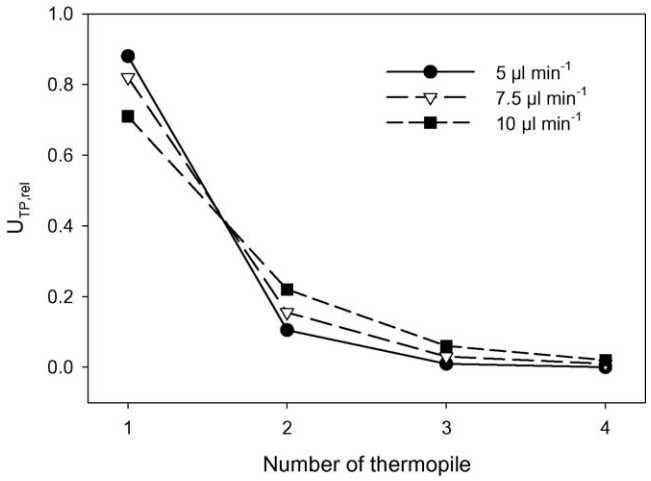

Fig. 3. Normalized steady-state signals of the four thermopiles measured for the TRIS protonation reaction with a 1.2 mm chamber. The data are normalized with respect to overall signal.

Table 2
Relative signals for different chamber heights

v (µl min^{-1})	h (mm)	TP1	TP2	TP3	TP4
7.5	1.2	0.82	0.15	0.03	0.005
	0.6	0.69	0.24	0.055	0.005
5	1.2	0.88	0.10	0.015	0
	0.6	0.81	0.16	0.02	0.005

0.6 mm according to the Einstein–Smoluchowski equation (diffusion coefficient $D_{H+} = 9.3e{-}9\ m^2\ s^{-1}$), i.e. the reaction should be completed already in the first segment even for a volume flow rate of 10 µl min^{-1}. This is much less than the experimental residence time of 2.4 min obtained for a flow rate of 10 µl min^{-1} and a 1.2 mm reaction chamber height.

The decrease of the chamber height reduces the residence time for a given flow rate. On the other hand, the path for mass and thermal diffusion is shortened which could partially compensate the residence time effect. An examination of the normalized signal of TP1 shows (Table 2) that a decrease of the residence time by factor 2.4 only results in a signal change of 10–20%. In the case of slow reactions the injection of reactant pulses with volumes smaller than the reaction chamber should be preferred in order to suppress heat loss and conversion errors [8].

3.2. Calorimetric sensitivity

The use of planar heat power detectors which are combined with distinct three-dimensional reaction chambers results in systematic errors, if integrated thin film heaters are applied for calibration. The errors are caused by incomplete heat power integration and the resulting sensitivity changes dependent on the position of the heat power dissipation. This is known from earlier investigations [9,10]. Therefore, chemical reactions have to be applied for calorimetric calibration. On the other hand, it was shown that the effective sensitivity can also be dependent on the kind of the reaction [14]. To understand more clearly the experimental conditions for well defined sensitivities and, hence, for maximal accuracy the presented study was performed.

In Table 3 the sensitivities of the thermopile segments for a simultaneously heat power dissipation in all segments are given. The sensitivities are related to the heat power generated inside the corresponding segment. The Joule heating data were obtained for water as chamber content. The smaller sensitivities in thermopile segments one and four can be explained by additional axial heat loss.

In Table 4 the sensitivities derived from Joule heating (chip heater) and BCHMP reaction are compared with those obtained from the TRIS protonization experiments. The presented Joule heating and BCHMP reaction based sensitivities are the mean values of thermopile segments two and three. For the TRIS protonization overall sensitivities were calculated by weighting signals of TP1 and TP2 corresponding to their lower sensitivities. Tables 3 and 4 indicate a decrease of the sensitivity with increasing chamber height. Furthermore, differences exist dependent on the local orientation of the laminar flows. In the case of 0.8 mm and 1.2 mm chambers and for vertical stacked flows the sensitivity is significantly larger if the HCl is located in the upper part of the reaction chamber. Probably maximum heat power dissipation is located nearer the detecting membrane due to the faster diffusion of the protons. Obviously the effect increases with the chamber height. For the 0.6 mm chamber no significant difference could be observed. Measurements with horizontal orientations (HA, HB, only for 1.2 mm chamber) also provided different sensitivities but in a much smaller extent. The mean of HA and HB is very close to that of VA and VB and it is also close to the sensitivity obtained with the BCHMP reaction. As it will be outlined in the next section the modeling of the heat transfer inside the chip module confirms that the observed differences in the sensitivities possibly are caused by non-homogeneous heat power dissipation inside the reaction chamber.

3.3. Modeling of the heat transfer

The model which we used for signal simulations was developed on the basis of the RC-analogy. Similar to the method described in Ref. [15] a set of MATLAB subroutines served

Table 3
Sensitivities of the thermopile segments based on chip heater and chemical heat power dissipation

Heat power source	h (mm)	S_{TP1} (V W^{-1})	S_{TP2} (V W^{-1})	S_{TP3} (V W^{-1})	S_{TP4} (V W^{-1})
Chip heater	0.6	7.5	8.3	8.3	7.3
	1.2	7.1	7.6	7.55	6.8
BCHMP	0.6	7.45	7.52	7.51	6.54
	1.2	4.88	5.39	5.53	4.79

Table 4
Sensitivities dependent on the chamber height and the local orientation of the laminar flows

h (mm)/mode	S_{TRIS} (V W^{-1})	S_{BCHMP} (V W^{-1})	S_{JH} (V W^{-1})	S_{calc} (V W^{-1})	SF_{mean}	SF_{upper}	SF_{lower}
0.6							
VA:	7.2	7.5	8.4	7.4	0.88	0.84	0.92
VB:	7.2						
0.8							
VA:	6.6	6.4	8.0	6.6	0.83	0.76	0.89
VB:	6.9						
1.2							
VA:	5.1	5.4	7.6	5.6	0.74	0.66	0.83
VB:	5.6						
HA:	5.2						
HB:	5.4						

S_{TRIS}, S_{BCHMP} and S_{JH}, experimental sensitivities from TRIS protonization, BCHMP reaction and Joule heating, respectively; S_{calc}, calculated sensitivity Eq. (4) using S_{JH} and SF_{mean}; SF_{mean}, SF_{upper} and SF_{lower}, correction factors for uniform heat power distribution, distribution inside the upper half part and distribution inside the lower half part.

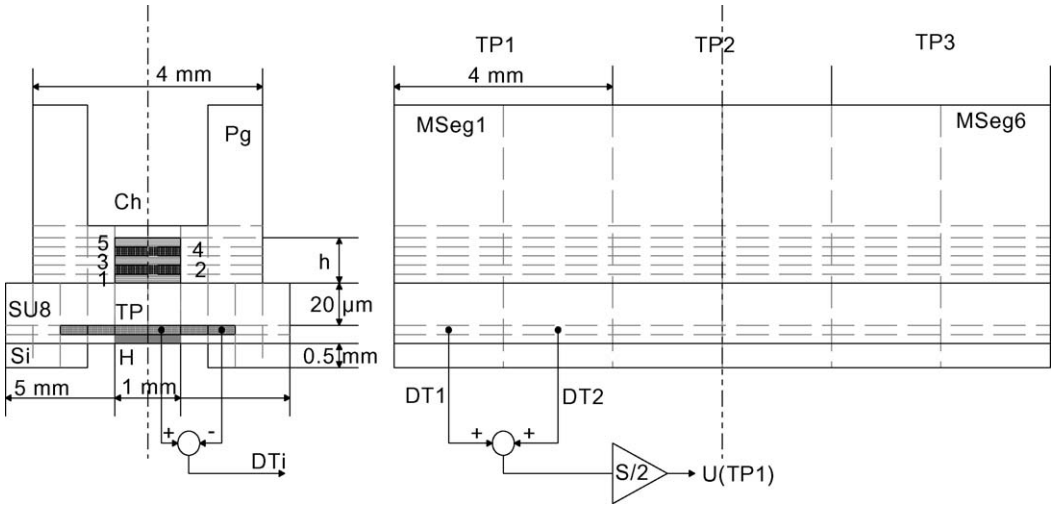

Fig. 4. Structure of the Model. The model consists of six segments (MSeg1–6) of identical structure. The elements of one segment are marked by dashed lines. Meaning of the symbols: Si, silicon wafer; SU8, epoxy glue; Pg, chamber material (PMMA); Ch, reaction channel; TP, thermopile material (300 nm); H, chip heater (30 nm); h, variable chamber height; DTi, temperature difference between hot and cold junction of segment i; S, sensitivity of one thermopile; U(TP1), output voltage of TP1; 1–5, virtual layers of the reaction channel (2, 3; position of the Pt heaters).

for a flexible design of the model. The structure of a simplified system which simulates sufficiently the signal generation is shown in Fig. 4. The system consists of six segments with 56 elements each. Each segment has the same structure. Two segments of the system describe one thermopile segment. From the experiments it was known that heat power dissipation in one thermopile segments does not effect significant temperature changes beyond the neighboring thermopile segments. Therefore, the six segments should be an adequately approximation of the calorimeter. In order to simulate the positional dependence of the sensitivity the reaction chamber was virtually split into five layers. The positions of the elements in which heat power is generated and from which the signals are obtained are marked (Fig. 4). To verify the model step response signals were simulated for different chamber heights and liquids and compared with the experimentally determined curves. For example, Fig. 5 shows the experimental and simulated thermopile signals for a 0.6 mm chamber and three different liquids. The heat was dissi-

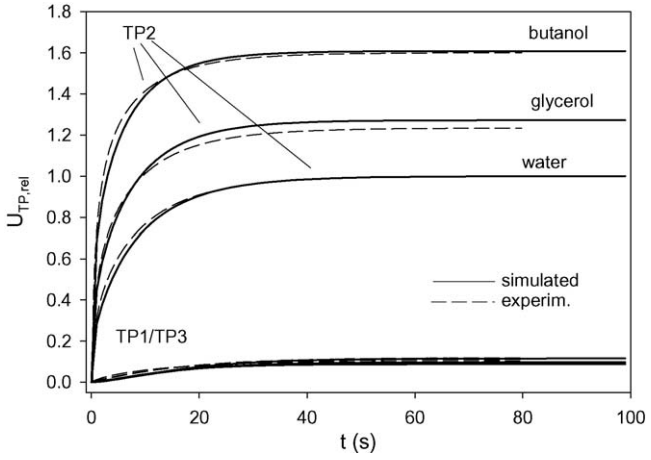

Fig. 5. Simulated and experimental step response for Joule heating in chip heater 2 and measured in thermopiles TP1/TP3 and TP2. Chamber height h = 0.6 mm. The signals are normalized with respect to the steady-state values of water.

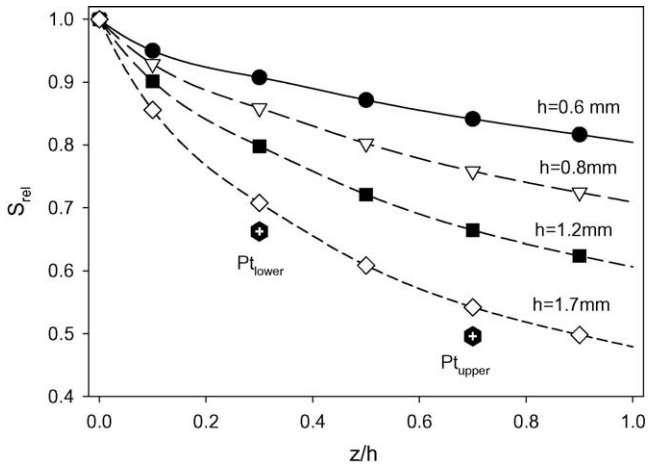

Fig. 6. Relative sensitivity inside the reaction chamber in vertical direction (z/h, relative distance to the membrane; h, chamber height). The sensitivities between the simulated values were interpolated by cubic splines.

pated by the chip heater in the central thermopile segment. The simulated and measured curves were normalized with respect to the water related steady-state values. From the comparisons of experimental and simulated signals one can draw the following conclusions: The dynamic behavior is well simulated. The relationship between signals from central and neighbor segments agrees with the experiment. The influence of the thermal properties of the liquids is well described. Larger deviations result for the variation of the channel height.

In order to study the positional dependency of the sensitivity step response signals were simulated for the heat power dissipation in the five virtual chamber layers (Fig. 5). After normalization with respect to the chip heater based signal the steady-state values provide a relative sensitivity $S_{rel}(z)$ as a function of the distance to the detector membrane z as it is depicted in Fig. 6. In Fig. 6 also the relative sensitivity values are shown, which were experimentally determined using the platinum wires. At least the tendency of the sensitivity change is well described by the model. If the relative sensitivity $S_{rel}(z)$ (sensitivity function) is known correction factors (shape factors SF, [8,11]) can be derived in order to improve sensitivity values obtained from Joule heating (S_{JH}):

$$S = S_{JH}\mathrm{SF} \tag{4}$$

In order to calculate the shape factor SF the local distribution of the heat power dissipation must be approximated. The shape factors enclosed in Table 4 were derived for three different heat power dissipations: $\mathrm{SF_{mean}}$, uniform dissipation in the complete chamber Eq. (5); $\mathrm{SF_{upper}}$, uniform dissipation in the upper half part of the chamber Eq. (6); $\mathrm{SF_{lower}}$, uniform dissipation in the lower half part of the chamber (Eq. (7)).

$$\mathrm{SF_{mean}} = \frac{1}{h}\int_{z=0}^{h} S_{rel}(z)\,\mathrm{d}z \tag{5}$$

$$\mathrm{SF_{upper}} = \frac{2}{h}\int_{z=h/2}^{h} S_{rel}(z)\,\mathrm{d}z \tag{6}$$

$$\mathrm{SF_{lower}} = \frac{2}{h}\int_{z=0}^{h/2} S_{rel}(z)\,\mathrm{d}z \tag{7}$$

The agreement of the sensitivity data calculated according Eq. (4) and the experimental ones (Table 4) seems to confirm that the decrease of the sensitivity with increasing chamber height is really caused by the sensitivity gradients inside the reaction chamber. Furthermore, the deviations of the shape factors depending on the local distribution of the heat power dissipation demonstrate that undefined heat power dissipation may produce errors if large chambers are used. Obviously, the latter was observed for the TRIS protonization at least in the 1.2 mm chamber.

3.4. External temperature perturbations

The influence of external temperature perturbations on the signal is dependent on the heat capacity of the sample and the container as well as the thermal time constant. Assuming a first order dynamic (localized heat capacity and thermal resistance, Fig. 7) a transfer function G(jω) according to Eq. (8) can be derived and then the frequency characteristic $A_f(\omega)$ for the transfer of temperature perturbations T_n to signal noise u_n can be expressed by Eq. (9) with the heat capacity of sample and container C and the time constant of the calorimeter τ. Because of the small time constants of chip calorimeters (in our case $\tau = 12$ s) the frequency characteristic increases nearly linear with the frequency of the temperature perturbations. Assuming white temperature noise of band width ω_B from Eq. (9) a relationship between voltage and temperature noise (rms) can be derived (Eq. (10)) [16].

$$G(\mathrm{j}\omega) = \frac{u_n(\mathrm{j}\omega)}{T_n(\mathrm{j}\omega)} = -S_p C\frac{\mathrm{j}\omega}{1+\mathrm{j}\omega\tau} \tag{8}$$

$$A_f(\omega) = \frac{|u_n(\mathrm{j}\omega)|}{|T_n(\mathrm{j}\omega)|} = S_p C\omega\frac{1}{\sqrt{1+\omega^2\tau^2}} \tag{9}$$

$$u_n \approx \frac{1}{\sqrt{3}} S_p C\omega_B T_n \tag{10}$$

In order to prove the noise transfer behavior we determined experimentally the frequency characteristic by generating stochastic temperature perturbations inside the thermostat. Based on simultaneously measured temperature and thermopile

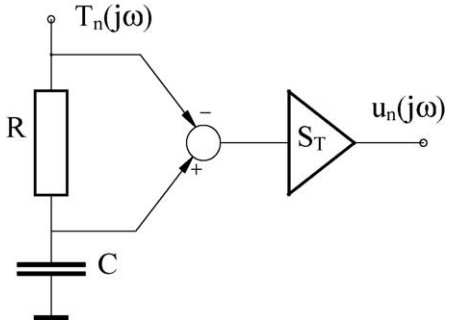

Fig. 7. RC model for the generation of signal noise u_n by ambient temperature perturbations T_n.

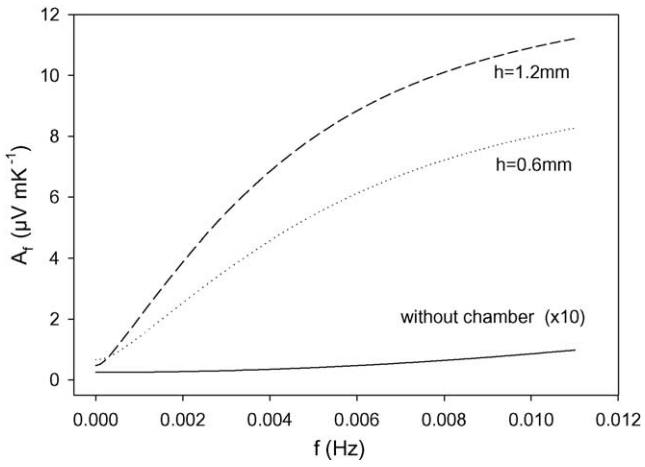

Fig. 8. Frequency characteristic $A_f(\omega)$ for the transfer of temperature perturbations to signal noise for different chamber heights.

signals a simple time-discrete ARX model [16] according to Eq. (11) was estimated by help of the system identification toolbox of MATLAB (MathWorks Inc., USA). The order $n = 8$ and $m = 8$ was chosen empirically.

$$u(t) + a_1 u(t - T_0) + \cdots + a_n u(t - nT_0) = b_1 T(t - T_0) + \cdots + b_m T(t - mT_0) \quad (11)$$

where T_0 is the sampling time, and n and m are the orders of the model.

From the models frequency characteristics were derived for calorimetric modules with different chamber heights. As shown in Fig. 8 the influence of the external temperature perturbations increases with the chamber size as expected. Considering the different sensitivities for $h = 0.6$ mm and $h = 1.2$ mm (5.4 V W^{-1} and 7.5 V W^{-1}, respectively) the doubling of the heat capacity is well reflected.

In Table 5 the measured voltage noise and the related heat power noise which are caused by the stochastic temperature perturbations are given for the three analyzed calorimetric modules. The increase with the chamber height is higher than expected regarding Eq. (10). The band width is not exactly the same. Further, no perfect white noise was generated. Despite of this one can deduce that a 100 µK noise level is sufficient to obtain a 50 nW resolution. In order to approach to the electronically determined limit of resolution (near 10 nW) a further improvement of the temperature control is necessary. On the other hand, the common mode rejection of a twin arrangement could be used to suppress temperature induced noise [14,17].

Table 5
Voltage noise u_n and related heat power noise p_n caused by ambient temperature perturbations of 0.8 mK and 0.01 Hz band width

$T_n = 0.8$ mK	$h = 0$ mm	$h = 0.6$ mm	$h = 1.2$ mm
u_n (µV)	0.5	2.5	6.9
p_n (µW)	0.05	0.34	1.3
p_n/T_n (W K^{-1})	7e−5	4e−4	1.6e−3

4. Conclusions

The miniaturization of calorimeters by help of silicon chip technology is advantageous for the investigation of fast reactions in small samples. If the interest is focused on slow and low energy processes like microbial activities or enzyme catalyzed reactions a decrease of the sample volume is accompanied by a reduced signal-to-noise ratio. Unfortunately, a possible gain in the signal-to-noise ratio by enlargement of the sample volumes is partially compensated due to a reduced average sensitivity and increasing temperature induced noise. Sensitivity gradients inside the reaction chamber which are caused by the planar geometry of the thermopile detectors also provoke systematic errors if non-uniform heat power distribution inside the reaction chamber is generated by the reaction. Therefore, the application of larger chambers is only possible if premixing of the reactants can be performed (see, e.g. Ref. [17]). Further, more effort for temperature control is necessary and increasing time constants degrade the dynamic performance of the calorimeter.

Acknowledgements

Financial support of the German Research Council (Deutsche Forschungsgemeinschaft, Wo576/5-3) and AiF (BMWA, AiF-Nr. 13328 BR) is gratefully acknowledged. The cooperation between Freiberg and Barcelona group was supported by integrated action (DAAD D/03/39344). Special thanks have to be addressed to Prof. Torra, UPC Barcelona, for helpful discussions. The stay of I.F. in TU Bergakademie Freiberg, was realized in the frame of SOCRATES program.

References

[1] F.E. Torres, P. Kuhn, D. de Bruyker, A.G. Bell, M.V. Wolkin, E. Peeters, J.R. Williamson, G.B. Anderson, G.P. Schmitz, M.I. Recht, S. Schweizer, L.G. Scott, H.J. Ho, S.A. Elrod, P.G. Schultz, R.A. Lerner, R.H. Bruce, PNAS 101 (2004) 9517–9522.
[2] M.Y. Efremov, F. Schiettekatte, M. Zhang, E.A. Olson, A.T. Kwan, R.S. Berry, L.H. Allen, Phys. Rev. Lett. 85 (2000) 3560.
[3] J. Lerchner, R. Kirchner, J. Seidel, D. Waehlisch, G. Wolf, Thermochim. Acta 415 (2004) 27.
[4] V. Baier, R. Föhdisch, A. Ihring, E. Kessler, J. Lerchner, G. Wolf, J.M. Köhler, M. Nietzsch, M. Krügel, Sens. Actuators A123–A124 (2005) 354–359.
[5] T. Maskow, J. Lerchner, M. Peitzsch, H. Harms, G. Wolf, J. Biotechnol. 122 (2006) 431–442.
[6] E.A. Johannessen, J.M.R. Weaver, L. Bourova, P. Svoboda, P.H. Cobbold, J.M. Cooper, Anal. Chem. 74 (2002) 2190–2197.
[7] Y. Zhang, S. Tadigadapa, Biosens. Bioelectron. 19 (2004) 1733–1743.
[8] J. Lerchner, A. Wolf, G. Wolf, V. Baier, E. Kessler, Thermochim. Acta, doi:10.1016/j.tca.2005.07.011.
[9] V. Torra, C. Auguet, J. Lerchner, P. Marinelli, H. Tachoire, Therm. Anal. Calorim. 66 (2001) 255–264.
[10] C. Auguet, J. Lerchner, P. Marinelli, F.J. Martorell, V. Torra, Therm. Anal. Calorim. 71 (2003) 951.
[11] J. Lerchner, G. Wolf, C. Auguet, V. Torra, Thermochim. Acta 382 (2002) 65.
[12] H.J. Buschmann, E. Schollmeyer, Thermochim. Acta 333 (1999) 49–53.
[13] M.A.A. O'Neill, A.E. Beezer, C. Labetoulle, L. Nicolaides, J.C. Mitchell, J.A. Or-chard, J.A. Connor, R.B. Kemp, D. Olomolaiye, Thermochim. Acta 399 (2003) 63–71.

[14] J. Lerchner, A. Wolf, R. Hüttl, G. Wolf, Chem. Eng. J. 101 (2004) 187–194.
[15] J. Lerchner, G. Wolf, C. Auguet, V. Torra, Thermochim. Acta 415 (2004) 9–13.
[16] L. Ljung, Systems Identification: Theory for the User, Prentice Hall, Englewood Cliffs, NJ, 1987.
[17] J. Higuera-Guisset, J. Rodriguez, M. Chacon, Thermochim. Acta 427 (2004) 187–191.